Chapter 16
An FE-BE Method for the Hydroelastic Vibration Analysis of Plates and Shells Partially in Contact with Fluid

I. Tugrul Ardic, M. Erden Yildizdag, and Ahmet Ergin

Abstract In this study, a combined finite element (FE)–boundary element (BE) method is presented to investigate the dynamic characteristics of shell and plate structures in contact with fluid. The numerical procedure consists of two parts. In the first part, the dynamic characteristics of structures are obtained under in-vacuo condition by using the finite element method. Then, in the second part, fluid-structure interaction effects are computed in terms of generalized added mass coefficients by using the boundary element method. In analyses, surrounding fluid is assumed ideal, i.e. inviscid, incompressible and irrotational, in the context of linear hydroelasticity theory. In order to show the applicability of the proposed method, the dynamic characteristics of two different structures —a vertical rectangular plate in contact with fluid on one side and a horizontal cylindrical shell partially filled with fluid— are investigated and compared with the results obtained with a commercial software, ANSYS.

16.1 Introduction

Vibration is one of the most important phenomena in engineering, and a broad range of studies investigating different aspects of vibrating structures can be found in literature (see, e.g., Alessandroni et al, 2005; Giorgio and Del Vescovo, 2019, 2018; Baroudi et al, 2019; Giorgio et al, 2017; Barchiesi et al, 2018; Abd-alla et al,

I. T. Ardic, M. E. Yildizdag, A. Ergin
Department of Naval Architecture and Ocean Engineering, Istanbul Technical University, Maslak, 34469, Istanbul, Turkey
e-mail: ardici@itu.edu.tr, yildizdag@itu.edu.tr, ergina@itu.edu.tr

M. E. Yildizdag
International Research Center for the Mathematics and Mechanics of Complex Systems, University of L'Aquila, Italy
e-mail: yildizdag@itu.edu.tr

B. E. Abali and I. Giorgio (eds.), *Developments and Novel Approaches in Nonlinear Solid Body Mechanics*, Advanced Structured Materials 130,
https://doi.org/10.1007/978-3-030-50460-1_16

2017; Cazzani et al, 2018; Bersani et al, 2016). Particularly, dynamic interaction between structures and their surrounding fluid media is of great concern in numerous engineering problems, e.g. vibration of water retaining structures (i.e. dam, storage tank, etc.) under earthquake loading, design of internal structures of nuclear reactors, structural designs in aerospace and shipbuilding industries. For a structure in contact with a fluid of comparable density, the presence of the fluid strongly affects the dynamic response behavior of the structure. This is one of the complex engineering problems, involving the determination of reactive forces due to induced pressure at fluid-structure interface as a result of transferring structural vibrations into fluid. As a special engineering discipline, hydroelasticity is known as a branch of science which is, as expressed in Bishop and Price (1979), concerned with the motion of deformable bodies through liquids.

Shells and plates have a wide range of applications as structural components in shipbuilding, aerospace and petrochemical industries. Therefore, accurate estimation of induced fluid loading on vibrating plates and shells is of practical importance to assess the reliability of these structural components under different circumstances. For a freely vibrating plate or shell, effect of interaction forces on the dynamic characteristics of the structure is relatively weak when the density of surrounding fluid is low, such as air. However, when the vibrating structure is in contact with a fluid of comparable density, such as water, fluid loading significantly alters the dynamic characteristics of the structure from those in vacuo. Therefore, motion of both the structure and fluid is strongly coupled.

Hydroelastic vibration of plates and shells has been extensively studied by many researchers. One of the pioneering studies in this field was presented by Warburton (1961). In his study, dynamic analysis of an infinitely long cylindrical shell submerged into infinitely deep fluid medium and/or filled with liquid was carried out analytically under the assumption that the mode shapes do not change both in air and when in contact with water. A fundamental work on fluid-coupled thin plates was performed experimentally by Lindholm et al (1965), with the aim of obtaining the wet dynamic characteristics (wet natural frequencies and corresponding wet mode shapes) of clamped rectangular plates submerged into fluid. In the study, the experiments were conducted to determine the wet dynamic characteristics of rectangular plates for different aspect ratios and submergence depths. Meyerhoff (1970) obtained the dynamic characteristics of a thin rectangular plate submerged in an incompressible and inviscid fluid by using dipole singularities to model fluid effects.

A number of analytical and semi-analytical methods have been conducted to predict elastic response of cylindrical shells in contact with fluid. For example, Chiba et al (1984a,b) and Goncalves and Ramos (1996) investigated the dynamic characteristics of partially liquid-filled, and clamped vertical cylindrical shells by using the Galerkin method. In both studies, cylindrical shells are clamped at the rigid bottom surface. Askari and Jeong (2010) studied a slightly different problem that a vertical cylindrical shell is clamped at the upper end and free at the bottom edge, and the dynamic characteristics of the fluid-coupled system was extracted by using the Rayleigh-Ritz method. Jeong and Lee (1996) carried out an analytical study based on Fourier series expansion to obtain natural frequencies of both partially liquid-

filled and partially submerged circular cylindrical shells. Jeong (1999) applied the same methodology to investigate the dynamic characteristics of cylindrical shells concentrically or eccentrically submerged in a rigid fluid container. Implementation of the wave propagation approach to solve acoustic wave equation was first applied by Zhang (2002) to study the dynamic behavior of submerged cylindrical shells. In this context, displacement fields of cylindrical shells are defined as traveling waves. Recently, the same approach was adopted by Zhang et al (2017) to analyze the free and forced vibration characteristics of fully-submerged elliptic cylindrical shells. In these studies, fluid medium is assumed to be compressible, inviscid and irrotational, and thus, the motion is governed by the Helmholtz equation, and shells are assumed to be infinitely submerged into fluid to neglect the free surface effects. When cylindrical shells are horizontally in contact with fluid, which is a typical configuration in many engineering problems, mathematical model become rather complex due to the lack of axial symmetry. This type of problem was first studied by Amabili and Dalpiaz (1995) and Amabili et al (1996), using experimental and semi-analytical methods, respectively. In the semi-analytical study, the solution of fluid problem was obtained analytically by the method of separation of variables, applying the infinite frequency limit boundary condition on the free surface. As done in the work of Jeong and Lee (1996), the radial displacements of the shell was defined by Fourier series expansion.

On the other hand, a lot of attempts have been made to investigate the dynamic characteristics of plates in contact with fluid using analytical approaches. In earlier studies, substantial simplifications have been made for analyzing rectangular and circular plates (see, e.g., De Espinosa and Gallego-Juarez, 1984; Kwak, 1991). Robinson and Palmer (1990) performed the modal analysis of a rectangular plate floating on the free surface of a stationary fluid under the assumptions of potential theory. Amabili et al (1996) investigated the free vibration of both circular and annular plates submerged into fluid, bounded with rigid walls and the free surface, including sloshing effects. Kwak (1997) calculated NAVMI (Non-dimensional Added Virtual Mass Incremental) factors for circular plates placed in an opening on the infinite rigid wall and in contact with fluid on one side. Cho et al (2014) investigated the free vibration characteristics of both bare and stiffened panels vertically in contact with stationary fluid. In this study, the kinetic and potential energy functionals of the system were obtained by superposing the energy components of the plate and stiffener, and the displacements of the plates were represented by orthogonal polynomials with Timoshenko beam function properties. The Rayleigh-Ritz method is often used to solve plate vibration problems due to its inherent advantage of being based on very general assumptions for obtaining optimal solutions with approximation properties of the trial spaces (see Amabili et al, 1996; Meylan, 1997; Jeong, 2003; Jeong and Kim, 2009; Liao and Ma, 2016; Datta and Jindal, 2019). For example, Kwak and Yang (2013) obtained the virtual added mass matrix of a partially immersed vertical rectangular plate in elliptical coordinates by using orthogonal Mathieu functions together with the Rayleigh-Ritz method. A theoretical model was developed by Askari et al (2013) to investigate the hydroelastic vibration of circular plates immersed in fluid by using the Rayleigh-Ritz method including the free surface effects. In the study, the compatibility conditions were satisfied both at the plate-liquid interface

and between the upper and lower liquid subdomains divided by plate. Then, the total velocity potential was defined as superposition of velocity potentials induced by the free surface and deformation of the plate, and the wet mode shapes were obtained by superposition of a finite number of admissible functions selected as dry mode shapes of the plate.

For structures with complex geometries such as mono- or multi-hull vessels, aircrafts, multi-purpose offshore structures and space vehicles, it is not possible to deal with the problem by using analytical approaches. Thus, alternative computational methods have been developed for the dynamic response analysis of such complex structures under the effect of fluid environment. In earlier studies, the finite element method (FEM) was recognized as a powerful numerical tool for the solution of fluid-structure interaction problems. In this direction, Zienkiewicz and Newton (1969) developed a method to solve fluid-structure interaction problems in which fluid and structure domains are both modeled with finite elements. In their method, fluid environment is governed by the acoustic wave equation, and fluid pressure acts as fundamental unknown in the matrix equations. The main drawback in this formulation is that the matrices are not symmetric. An alternative FEM formulation, in which the fluid displacement is main unknown instead of pressure, is developed by Kalinowski (1974) to take the advantage of symmetric matrices. Following these two seminal papers, FEM has been successfully applied in hydroelastic vibration problems, dealing with various structures such as rectangular plates (Marcus, 1978; Motley et al, 2013), spherical shells (Liang et al, 2001), steelworks in fluid-carrying vessels (Volcy et al, 1980) and stiffened cylindrical shells (Hsu and Jen, 2010). One of the major drawbacks in FEM approaches is that, when the structure vibrates in an unbounded fluid environment, the entire geometry including surrounding fluid region must be discretized with finite elements. Clearly, this situation leads to a considerable increase in the number of elements and computation time. In order to overcome this difficulty, Fu and Price (1987) developed a hybrid model in which the structural problem is handled by FEM and the fluid problem by the boundary element method (BEM). Dealing with the fluid problem by using BEM, as discretization is only performed over the wetted surface of the structure, instead of the entire surrounding fluid, the method provides a substantial advantage in terms of computation time. In order to take the advantage of this approach, several researchers investigated hydroelastic vibration problems of different geometries (see Junge et al, 2011; Zheng et al, 2017). For example, Ergin and Temarel (2002) used a combined FE-BE method to calculate the free vibration characteristics of thin circular cylindrical shells in contact with internal and external liquid. In this study, it was pointed out that the mode shapes of the cylindrical shell partially in contact with fluid differed significantly from those obtained under in-vacuo condition. The same methodology adopted by Ergin and Uğurlu (2003) to calculate natural frequencies and corresponding mode shapes of clamped rectangular plates both in-vacuo and in contact with fluid. Recently, Yildizdag et al (2019) examined the hydroelastic vibration characteristics of the same plate immersed in fluid in vertical and horizontal positions, respectively, by using an isogeometric FE-BE approach.

The central theme of this study is to present a general numerical strategy for investigating natural frequencies and corresponding mode shapes of plate and shell structures partially in contact with fluid. The fluid environment is considered within the context of potential theory, i.e., fluid is inviscid, incompressible, and its motion is irrotational. By assuming that the structure vibrates with a relatively high frequency and the corresponding fluid pressure is in phase with the structural acceleration, the linearized fluid-structure interaction system is established, and generalized fluid-structure interaction forces are derived from the linear form of the Bernoulli equation. By using this linearized hydroelasticity theory, the fluid-structure interaction problem may be divided into in-vacuo (dry) and wet parts, and each problem can be analyzed separately. In the absence of any external force and structural damping, the in-vacuo part of the analysis is performed by solving the equation of motion with FEM. The surface normal velocity components of the fluid on the wetted part of the structure are obtained by applying continuity condition, in other words, the normal velocities on the wetted surface are expressed in terms of in-vacuo modal displacements. In the wet part of the analysis, BEM is applied to obtain hydrodynamic forces associated with each principle mode. The wetted surface is discretized with boundary elements (hydrodynamic panels), with a point source of constant strength placed at the geometric center of each panel. In the absence of axial flow, free surface waves and viscous effects, the interaction between the structure and fluid takes place only through the inertial effect of fluid (added mass coefficients). Therefore, the total generalized mass matrix, which is formed by merging the generalized structural mass and hydrodynamic added mass matrices, is used to solve the eigenvalue problem for the fluid-structure system. The numerical framework presented here is applied to two specific geometries: a rectangular plate and a horizontal cylindrical shell, partially in contact with fluid. In order to assess the validity and accuracy of the method, wet natural frequencies and corresponding mode shapes are compared with those obtained by commercially available finite element program, ANSYS (2013).

16.2 Mathematical Model

16.2.1 In-Vacuo (Dry) Structural Analysis

In the absence of structural damping and external forces, motion of the structure can be defined by

$$\mathbf{M}\ddot{\mathbf{x}}(t) + \mathbf{K}\mathbf{x}(t) = \mathbf{0} \tag{16.1}$$

where $\mathbf{M}$ is the structural mass matrix and $\mathbf{K}$ is the structural stiffness matrix. Here, $\ddot{\mathbf{x}}$ and $\mathbf{x}$ are the acceleration and displacement vectors of the structure, respectively. By assuming the structure oscillates harmonically in time, a trial solution can be express as follows

$$\mathbf{x} = \mathbf{u}e^{i\omega t} \tag{16.2}$$

where $\mathbf{u}$ represents the amplitude vector of the displacements, and ω is the frequency of oscillation. By using this expression, Eq. (16.1) takes the following form

$$\left(-\omega^2\mathbf{M} + \mathbf{K}\right)\mathbf{u} = \mathbf{0}. \tag{16.3}$$

Eq. (16.3) defines an eigenvalue problem, and the non-trivial solutions of this system can only be obtained when the following condition is satisfied,

$$\det\left[-\omega^2\mathbf{M} + \mathbf{K}\right] = 0. \tag{16.4}$$

Here, Eq. (16.4) is called characteristic equation, or frequency equation. For a structure having N degrees of freedom, the characteristic equation possesses N distinct roots, $\omega_1^2, \omega_2^2, ..., \omega_n^2$, and the square roots of these quantities represent the natural frequencies of the structure. For every frequency, ω_r, there is a corresponding vector of amplitudes, $\mathbf{u}_r$. The eigenvector $\mathbf{u}_r$ corresponding to the natural frequency ω_r denotes the r-th principal modal vector.

Based on orthogonality of modal vectors, a vector space consisting of modal vectors can be formed and the response of the system can be defined by superposition of the displacements in the principal modes

$$\mathbf{U} = \sum_{r=1}^{N} D_r p_r(t) = \mathbf{D}\,\mathbf{p}(t) \tag{16.5}$$

where $\mathbf{D}$ and $\mathbf{p}$ are $N \times N$ modal matrix consisting of modal vectors and $N \times 1$ column vector representing the principal modes, respectively. Substituting Eq. (16.5) into Eq. (16.3) and multiplying by $\mathbf{D}^T$, the equation of motion is obtained in terms of the principal coordinates of the structure

$$\left(-\omega^2\mathbf{a} + \mathbf{c}\right)\mathbf{p} = \mathbf{0}. \tag{16.6}$$

Here, $\mathbf{a}$ and $\mathbf{c}$ denote the generalized mass and stiffness matrices, respectively, and they are $\mathbf{a} = \mathbf{D}^T\mathbf{M}\,\mathbf{D}$ and $\mathbf{c} = \mathbf{D}^T\mathbf{K}\,\mathbf{D}$, respectively.

One of the useful and important features of modal vectors is that they are orthogonal. This is to say that:

$$\begin{aligned} &\mathbf{u}_s^T\mathbf{K}\,\mathbf{u}_r = 0 && \text{if } r \neq s, \\ &\mathbf{u}_s^T\mathbf{K}\,\mathbf{u}_r = \omega_r^2 a_{rr} && \text{if } r = s, \end{aligned}$$

and

$$\begin{aligned} &\mathbf{u}_s^T\mathbf{M}\,\mathbf{u}_r = 0 && \text{if } r \neq s, \\ &\mathbf{u}_s^T\mathbf{M}\,\mathbf{u}_r = a_{rr} && \text{if } r = s. \end{aligned}$$

16.2.2 Wet Analysis

16.2.2.1 Formulation of the Fluid Problem

By assuming the fluid is ideal, i.e. inviscid and incompressible, and its motion is irrotational, there exists a fluid velocity vector, $\mathbf{v}(x, y, z)$, defined as the gradient of the velocity potential function, $\phi(x, y, z)$, satisfies the Laplace's equation,

$$\nabla^2 \phi(x, y, z) = 0. \tag{16.7}$$

For a system under fluid-structure interaction effects, the Laplace equation defines a boundary value problem. Therefore, boundary conditions must be defined over the entire wetted surface of the elastic body and also on the free surface. There is no fluid transfer in the direction perpendicular to the wetted surface of the elastic structure. As a result, the normal fluid velocity must be equal to the normal velocity on the structure and this condition for the r-th modal vibration of the elastic structure in contact with a quiescent fluid can be expressed as

$$\frac{\partial \phi_r}{\partial \mathbf{n}} = \mathbf{u}_r \cdot \mathbf{n} \qquad \text{on } S_w. \tag{16.8}$$

Here, $\mathbf{n}$ is the unit normal vector on the wetted surface, S_w, and $\mathbf{u}_r$ is the r-th modal displacement vector of the median surface of the structure. Furthermore, it is assumed that the structure vibrates at relatively high frequencies; thus, the effect of free surface waves due to the modal distortions of the structure is neglected in the mathematical model. Thus, the free surface boundary condition is simplified and expressed as follows

$$\phi_r = 0, \quad \text{on the free surface.} \tag{16.9}$$

In this study, the free surface boundary condition given in Eq. (16.9) is satisfied by using the image method (Kito, 1970). For this purpose, an imaginary surface is introduced by mirroring the wetted part of the structure by taking the free surface as mirror plane, and the modal displacements over the wetted surface are also mirrored, as described in Fig. 16.1. Hence, by utilizing the image method, the fluid-structure interaction problem is reduced to classical Neumann problem.

16.2.2.2 Numerical Evaluation of Perturbation Potential

The boundary integral equation formulation for a three-dimensional inviscid flow, due to time-harmonic oscillating structure, can be expressed by unknown source strength, ϕ^*, over the wetted and image surfaces.

$$c\phi(P) = \iint\limits_{S_w+S_i} q(Q)\phi^*(P, Q)\, ds - \iint\limits_{S_w+S_i} \phi(Q)\, q^*(P, Q)\, ds \tag{16.10}$$

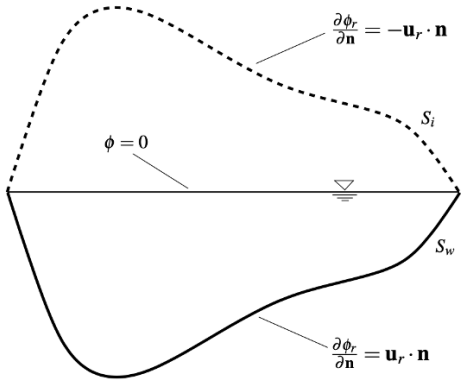

Fig. 16.1 Wetted surface and its image.

where ϕ^* is the fundamental solution for the velocity potential. Here, c is a space-angle constant and it is 0.5 for constant-strength source panels. The integral equation, Eq. (16.10), allows us to calculate unknown velocity potential $\phi(Q)$ both over the wetted boundary and inside the fluid domain when the flux $q(Q)$ is known. In this equation, Q and P represent the field and load points on the wetted and imaginary surfaces, respectively, and $S_w + S_i$ denotes the total wetted and imaginary surfaces. The fundamental solution of the Laplace operator, ϕ^*, and the cartesian components of its gradient, q^*, are given for 3-D case, respectively, as

$$\phi^*(P,Q) = \frac{1}{4\pi r}, \tag{16.11}$$

$$q_x^* = -\frac{r_{,x}}{4\pi r^2}, \qquad q_y^* = -\frac{r_{,y}}{4\pi r^2}, \qquad q_z^* = -\frac{r_{,z}}{4\pi r^2} \tag{16.12}$$

where r is the Euclidean distance,

$$r = \sqrt{(x_Q - x_P)^2 + (y_Q - y_P)^2 + (z_Q - z_P)^2}, \tag{16.13}$$

between the source and field points. Here, $r_{,x}$, $r_{,y}$ and $r_{,z}$ are the projections of the Euclidean distance, r, on the x, y and z axes, respectively, and expressed as follows

$$r_{,x} = \frac{x_Q - x_P}{r}, \quad r_{,y} = \frac{y_Q - y_P}{r}, \quad r_{,z} = \frac{z_Q - z_P}{r}. \tag{16.14}$$

The integral equation in Eq. (16.10) is a Fredholm equation of the second kind, and it must be satisfied over the wetted and imaginary surfaces of the elastic body. This equation can be numerically solved by dividing the wetted and imaginary surfaces of the structure into hydrodynamic panels, and the flux and unknown velocity potential are taken as constant over each panel. In this framework, the numerical solution of Eq. (16.10) is satisfied only at the geometric center of each panel. Therefore,

the surface integrals in Eq. (16.10) may be written as the sum of integrals over N constant-strength quadrilateral panels

$$\frac{1}{2}\phi_i = -\sum_{j=1}^{N} q^* \, \phi_j + \sum_{j=1}^{N} \phi^* \, q_j. \tag{16.15}$$

In Eq. (16.15), it is assumed that all q_j values are obtained from the in-vacuo (dry) analysis (each column of the matrix $\mathbf{D}$ is defined in Eq. (16.5)), and therefore, the corresponding unknown source strengths at each panel, ϕ_j, are calculated from the solution of Eq. (16.15) for each principal mode shape.

16.2.2.3 Generalized Fluid-Structure Interaction Forces

Generalized fluid-structure interaction forces are calculated by using the pressure distribution on the wetted surface, obtained by solving the potential flow problem. The r-th component of the generalized fluid-structure interaction force due to k-th modal vibration can be obtained by using the following equation

$$Z_{rk} = \iint_{S_w} P_k \mathbf{u}_r \cdot \mathbf{n} \, ds. \tag{16.16}$$

The fluid pressure acting on the wetted surface of the structure due to the k-th modal vibration can be calculated using the linearized form of the Bernoulli equation,

$$P_k = \omega^2 \rho \phi_k. \tag{16.17}$$

Thus, the r-th component of the generalized fluid-structure interaction force amplitude due to the k-th modal vibration takes the following form

$$Z_{rk} = \iint_{S_w} (\omega^2 \rho \phi_k) \mathbf{u}_r \cdot \mathbf{n} \, ds, \tag{16.18}$$

and then the generalized added mass term, A_{rk}, can be expressed as follows

$$A_{rk} = \frac{\rho}{\omega^2} \iint_{S_w} \omega^2 \phi_k \mathbf{u}_r \cdot \mathbf{n} \, ds. \tag{16.19}$$

If the k-th principal coordinate is in the form of $p_k(t) = p_k e^{i\omega t}$, then the r-th component of the generalized fluid-structure interaction force can be written as

$$Z_{rk} = A_{rk} \omega^2 p_k e^{i\omega t} = -A_{rk} \ddot{p}_k. \tag{16.20}$$

16.2.2.4 Calculation of Wet Frequencies and Mode Shapes

Fluid-structure interaction forces acting on a freely vibrating structure in the vicinity of a free surface vary with frequency. In this study, it is assumed that the structure vibrates with a relatively high frequency, thus the generalized added mass is constant and independent of vibration frequency. The generalized equation of motion may therefore be written as

$$\left[-\omega^2(\mathbf{a}+\mathbf{A})+\mathbf{c}\right]\mathbf{p}_0=\mathbf{0} \tag{16.21}$$

where $\mathbf{c}$ and $\mathbf{a}$ denote the generalized structural stiffness and generalized mass matrices, respectively. The $M \times M$ matrix $\mathbf{A}$ represents the frequency-independent generalized added mass matrix. By solving the eigenvalue problem expressed in Eq. (16.21), one can obtain each wet natural frequency, ω_k, and corresponding eigenvector $\mathbf{p}_{0_k}=\{p_{k_1}, p_{k_2}, ..., \mathbf{p}_{k_M}\}$. The wet mode shapes of the structure can be defined as superposition of the dry modes, where the contribution of the j-th mode is represented by p_{k_j},

$$\mathbf{q}_k(x,y,z)=\sum_{j=1}^{M}\mathbf{u}_j(x,y,z)\,\mathbf{p}_{k_j} \tag{16.22}$$

where M denotes the number of modes considered in the analysis. It should be noted that the fluid-structure interaction forces associated with the inertial effect of the fluid do not have the same spatial distribution as those of the in-vacuo modal forms. As a consequence, this produces hydrodynamic coupling between in-vacuo modes.

16.3 Numerical Examples

In this section, the presented FE-BE procedure is applied to two different structures (rectangular plate and cylindrical shell) in contact with fluid, in order to demonstrate the applicability of the method. In the numerical examples, flat shell elements are adopted to conduct the in-vacuo analyses. The FEM formulation of flat shell elements used in this study can be found in Appendix.

16.3.1 Vertical Rectangular Plate in Contact with Fluid on One Side

The proposed mathematical model is first applied to a rectangular plate partially in contact with fluid on one side and clamped along its all edges (see Fig. 16.2). The rectangular plate has the length $\ell = 2.0$ m, height $h = 1.4$ m and thickness $t = 10$

mm. The plate is made of steel with the following material properties: Young's Modulus, $E = 206$ GPa, Poisson's Ratio, $\nu = 0.3$, and density, $\rho_s = 7850\ \mathrm{kg/m^3}$. The density of surrounding fluid is $\rho_f = 1025\ \mathrm{kg/m^3}$, and d denotes the submerging depth.

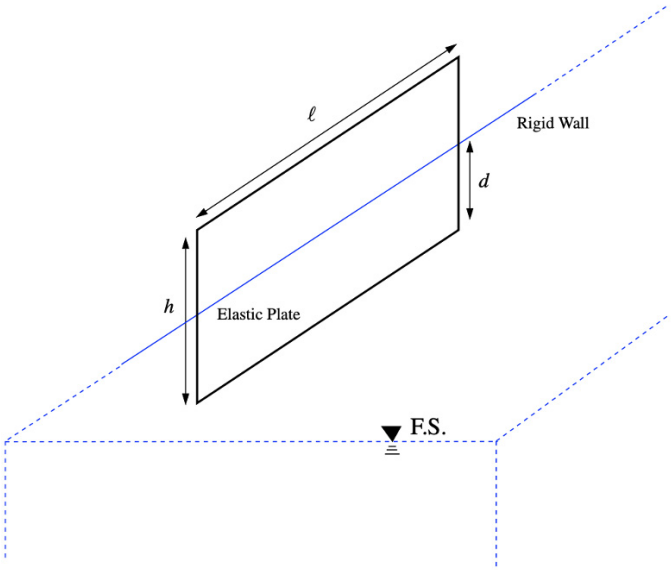

Fig. 16.2 Vertical cantilever plate in contact with fluid on one side.

In the first part of the analysis (i.e. dry analysis), natural frequencies and corresponding mode shapes under in-vacuo condition are obtained by solving the equation of motion. The results obtained by the present method are compared with those calculated using a commercial finite element software, ANSYS. In order to show the convergence of the first six natural frequency values, the structure was discretized by 300, 588, and 972 elements, respectively. The calculated frequency values are shown in Table 16.1 for the first six dry modes. The presented results clearly show that the differences between the calculated values in the 2nd and 3rd idealizations are negligible.

Moreover, the first six in-vacuo mode shapes of the rectangular plate are shown in Fig. 16.3. As expected, the complexity of the modal configurations increases with increasing frequency. These mode shapes may be classified into two groups, as symmetric and antisymmetric with respect to the axis passing through the longitudinal center of the plate. With this respect, the 1st, 3rd, 4th and 6th modes are symmetric, and the 2nd and 5th modes are antisymmetric. In Table 16.2, S and A stand for symmetry and antisymmetry, respectively.

Table 16.1 Convergence of dry natural frequencies (Hz).

Mode	This study			ANSYS
	300 El.	588 El.	972 El.	7500 El.
1 (S)	34.69	34.74	34.76	34.78
2 (S)	55.27	55.43	55.49	55.56
3 (A)	83.65	83.77	83.83	83.83
4 (S)	89.77	90.04	90.16	90.25
5 (A)	102.21	102.68	102.87	103.06
6 (S)	133.96	124.01	135.72	135.72

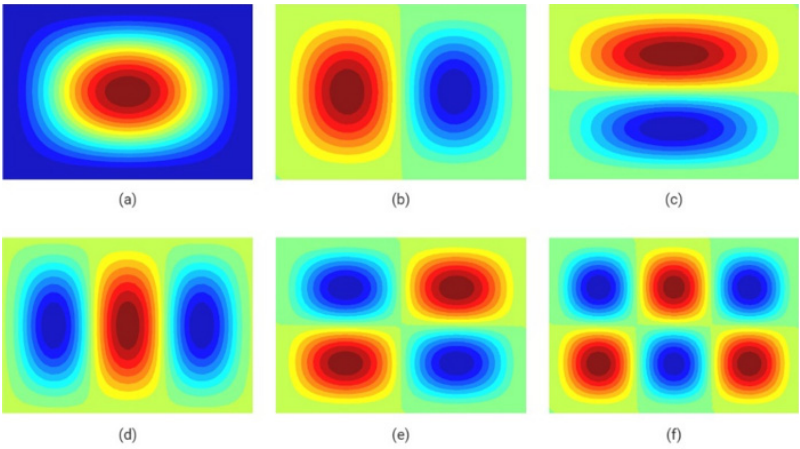

Fig. 16.3 In-vacuo mode shapes of rectangular plate: (a) 1st mode (34.76 Hz); (b) 2nd mode (55.49 Hz); (c) 3rd mode (83.83 Hz); (d) 4th mode (90.16 Hz); (e) 5th mode (102.87 Hz); (f) 6th mode (135.29 Hz).

In the second part of the analysis (i.e. wet analysis), wet natural frequencies and corresponding mode shapes of the rectangular plate are obtained for four different submerging ratios, namely $d/h = 0.25, 0.50, 0.75, 1.00$. The results obtained by the proposed FE-BE procedure are compared with those obtained by ANSYS. In ANSYS, the rectangular plate is discretized with four-node quadrilateral SHELL181 elements, and the surrounding fluid domain is modeled by FLUID30 elements. The density and sonic velocity are 1025 kg/m^3 and 1507 m/s, respectively. As the structure vibrates in high-frequency region, the infinite frequency limit condition is imposed on the free surface of fluid ($\phi = 0$).

In Table 16.2, a convergence study is presented for the wet frequencies obtained by using the proposed FE-BE procedure. In this study, for each submerging depth ratio (d/h), three different panel idealizations are adopted, and the results are compared with those obtained using ANSYS. The number of hydrodynamic panels adopted over the wetted surface, respectively, is 145, 344 and 580 for $d/h = 0.25$; 290,

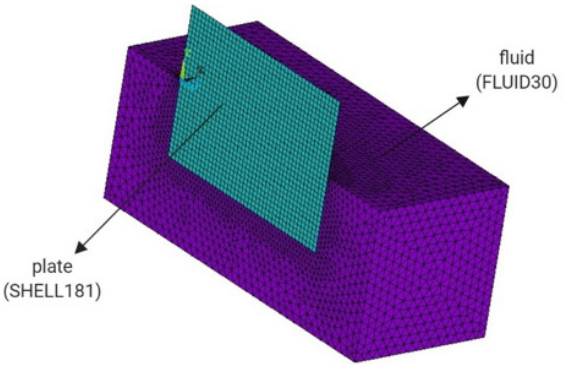

Fig. 16.4 ANSYS model of vertical plate in contact with fluid ($d/h = 0.5$).

645 and 1160 for $d/h = 0.50$; 435, 990 and 1740 for $d/h = 0.75$; 580, 1290 and 2320 for $d/h = 1.00$. As expected, the wet natural frequencies are lower than the corresponding in-vacuo frequencies. Difference between in-vacuo and wet natural frequencies is significant for the submerging depth ratio $d/h = 1.00$. As it is observed from Table 16.2, differences between the 2nd and 3rd idealizations for all submerging depth ratios are negligible. In addition, the converged values compare perfectly well with those of ANSYS. The maximum differences between the 3rd idealization and ANSYS which correspond to the first modes are 2.4%, 1.6% and 3.7% for submerging depth ratios $d/h = 0.25, 0.50$ and 1.00, respectively, while,

Table 16.2 Convergence of wet natural frequencies (Hz) for submerging depth ratios $d/h = 0.25$, 0.50, 0.75 and 1.00.

Mode	This study			ANSYS
	145 El.	344 El.	580 El.	881000 El.
1 (S)	33.17	33.19	33.19	33.99
2 (S)	54.19	54.21	54.22	54.18
3 (A)	76.23	76.29	76.30	76.33
4 (S)	87.70	87.71	87.71	87.71
5 (A)	94.05	94.06	94.06	93.94
6 (S)	124.09	124.01	123.96	123.67

(a) $d/h = 0.25$

Mode	This study			ANSYS
	290 El.	645 El.	1160 El.	938000 El.
1 (S)	22.66	22.65	22.63	22.99
2 (S)	37.98	37.91	37.87	37.79
3 (A)	61.07	60.92	60.86	60.51
4 (S)	63.91	63.73	63.65	63.66
5 (A)	80.37	80.22	80.16	80.09
6 (S)	97.75	97.22	96.99	96.80

(b) $d/h = 0.50$

Mode	This study			ANSYS
	435 El.	990 El.	1740 El.	968000 El.
1 (S)	15.46	15.43	15.41	15.39
2 (S)	28.46	28.37	28.33	28.21
3 (A)	49.18	49.01	48.93	48.11
4 (S)	64.64	64.38	64.26	64.14
5 (A)	0.000	0.000	0.516	0.000
6 (S)	83.20	82.69	82.48	82.38

(c) $d/h = 0.75$

Mode	This study			ANSYS
	580 El.	1290 El.	2320 El.	1616500 El.
1 (S)	13.28	13.24	13.22	12.73
2 (S)	26.02	25.88	25.82	25.52
3 (A)	42.86	42.53	42.40	41.56
4 (S)	47.73	47.32	47.15	46.59
5 (A)	56.56	56.02	55.80	55.41
6 (S)	79.71	78.73	78.33	77.61

(d) $d/h = 1.00$

for submerging depth ratio $d/h = 0.75$, the maximum difference (1.7%) is obtained for the 3rd mode.

In Table 16.3, the generalized added mass coefficients, for submerging depth ratios $d/h = 0.25, 0.50, 0.75$ and 1.00, are presented for the first 8 distortional mode shapes (five symmetric and three antisymmetric). The generalized added mass coefficients are scaled to a generalized mass of 1kg m^2. The off-diagonal terms given in the table represent the hydrodynamic coupling between in-vacuo modes. It is clear that all the coefficients increase with increasing submerging depth ratio, due to increase in wetted surface area. It can also be observed that the hydrodynamic coupling is strong between symmetric modes itselves as well as antisymmetric modes. However, the coupling between these two mode groups are negligible. In particular, strong coupling can be observed between 1st and 3rd symmetric as well as 2nd and 5th antisymmetric modes for submerging depth ratio $d/h = 0.50$. The diagonal terms are dominant compared to the off-diagonal terms, especially for submerging depth ratios 0.75 and 1.00.

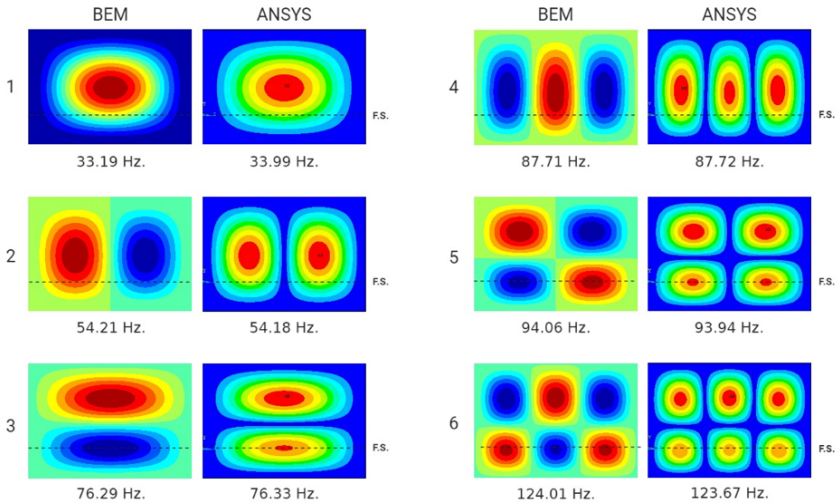

Fig. 16.5 Natural frequencies and associated modes of rectangular plate for submerging depth ratio $d/h = 0.25$.

Figs. 16.5-16.8 show the calculated wet mode shapes and wet frequencies for $d/h = 0.25, 0.50.0.75$ and 1.00, respectively. In order to obtain the wet mode shapes, the generalized added mass matrix is first formed by solving Eq. (16.19). Then, the eigenvalue problem expressed in Eq. (16.21) is solved for obtaining wet natural frequencies and corresponding mode shapes. A maximum number of $M = 24$ in-vacuo modes was adopted in computations.

It is clear that the differences between in-vacuo and wet mode shapes are noticeable, especially for higher submerging depth ratios (0.5 and higher). It can also be

Table 16.3 Generalized added mass coefficients (kg m^2) for rectangular plate partially submerged in fluid.

Mode	1 (S)	2 (A)	3 (S)	4 (S)	5 (A)	6 (S)	7 (A)	8 (S)
1 (S)	0.05	0.00	0.09	0.00	0.00	0.00	0.00	-0.13
2 (A)	0.00	0.05	0.00	0.00	0.09	0.00	0.00	0.00
3 (S)	0.09	0.00	0.19	0.00	0.00	0.00	0.00	-0.26
4 (S)	0.00	0.00	0.00	0.05	0.00	-0.09	0.00	0.01
5 (A)	0.00	0.09	0.00	0.00	0.18	0.00	0.00	0.00
6 (S)	0.00	0.00	0.00	-0.09	0.00	0.18	0.00	-0.01
7 (A)	0.00	0.00	0.00	0.00	0.00	0.00	0.05	0.00
8 (S)	-0.13	0.00	-0.26	0.01	0.00	-0.01	0.00	0.36

(a) $d/h = 0.25$

Mode	1 (S)	2 (A)	3 (S)	4 (S)	5 (A)	6 (S)	7 (A)	8 (S)
1 (S)	1.11	0.00	1.24	-0.06	0.00	0.03	0.00	0.56
2 (A)	0.00	0.94	0.00	0.00	1.02	0.00	0.06	0.00
3 (S)	1.24	0.00	1.58	-0.11	0.00	0.09	0.00	1.02
4 (S)	-0.06	0.00	-0.11	0.81	0.00	-0.85	0.00	-0.08
5 (A)	0.00	1.02	0.00	0.00	1.27	0.00	0.10	0.00
6 (S)	0.03	0.00	0.09	-0.85	0.00	1.04	0.00	0.09
7 (A)	0.00	0.06	0.00	0.00	0.10	0.00	0.70	0.00
8 (S)	0.56	0.00	1.02	-0.08	0.00	0.09	0.00	1.09

(b) $d/h = 0.50$

Mode	1 (S)	2 (A)	3 (S)	4 (S)	5 (A)	6 (S)	7 (A)	8 (S)
1 (S)	3.78	0.00	-1.39	0.35	0.00	-0.15	0.00	0.02
2 (A)	0.00	2.77	0.00	0.00	0.85	0.00	0.29	0.00
3 (S)	-1.39	0.00	2.18	-0.22	0.00	0.14	0.00	0.97
4 (S)	0.35	0.00	-0.22	2.20	0.00	-0.60	0.00	-0.05
5 (A)	0.00	0.85	0.00	0.00	1.70	0.00	0.15	0.00
6 (S)	-0.15	0.00	0.14	-0.60	0.00	1.41	0.00	0.09
7 (A)	0.00	0.29	0.00	0.00	0.15	0.00	1.76	0.00
8 (S)	0.02	0.00	0.97	-0.05	0.00	0.09	0.00	1.43

(c) $d/h = 0.75$

Mode	1 (S)	2 (A)	3 (S)	4 (S)	5 (A)	6 (S)	7 (A)	8 (S)
1 (S)	5.59	0.00	0.47	0.70	0.00	0.12	0.00	0.86
2 (A)	0.00	3.63	0.00	0.00	0.13	0.00	0.49	0.00
3 (S)	0.47	0.00	2.94	0.13	0.00	0.15	0.00	0.28
4 (S)	0.70	0.00	0.13	2.76	0.00	0.08	0.00	0.19
5 (A)	0.00	0.13	0.00	0.00	2.42	0.00	0.05	0.00
6 (S)	0.12	0.00	0.15	0.08	0.00	2.02	0.00	0.06
7 (A)	0.00	0.49	0.00	0.00	0.05	0.00	2.12	0.00
8 (S)	0.86	0.00	0.28	0.19	0.00	0.06	0.00	2.11

(d) $d/h = 1.00$

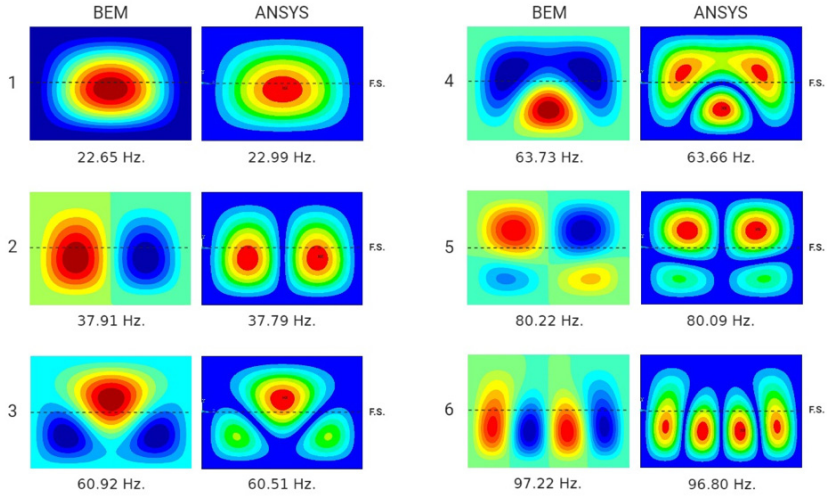

Fig. 16.6 Natural frequencies and associated modes of rectangular plate for submerging depth ratio $d/h = 0.50$.

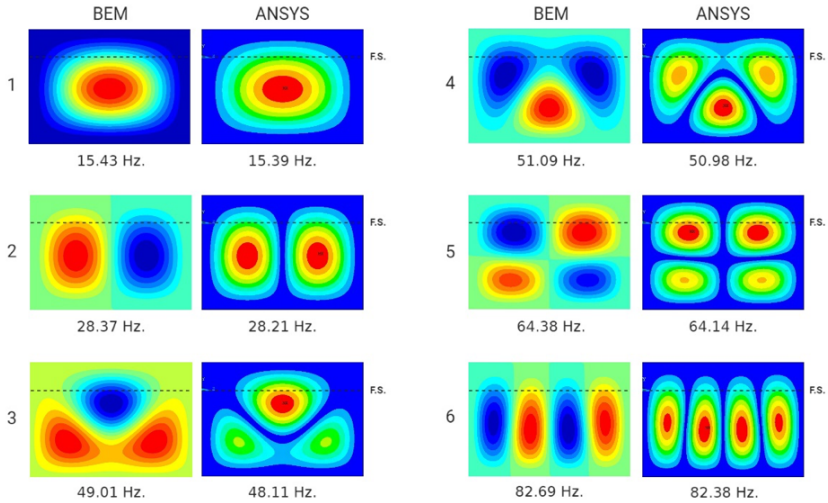

Fig. 16.7 Natural frequencies and associated modes of rectangular plate for submerging depth ratio $d/h = 0.75$.

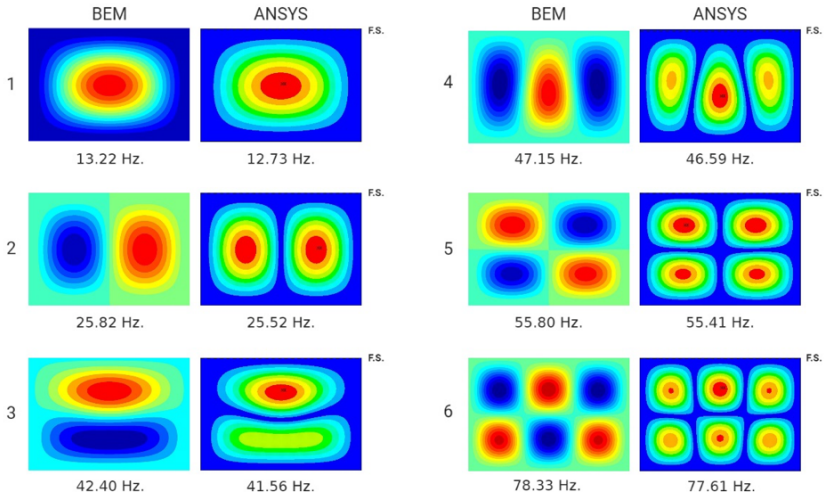

Fig. 16.8 Natural frequencies and associated modes of rectangular plate for submerging depth ratio $d/h = 1.00$.

said that the maximum difference, compared to those in vacuo, occurs for submerging depth ratios $d/h = 0.5$ and 0.75. For all the depth ratios, changes in the first and second wet modes are insignificant, compared to the higher ones. In general these two fundamental mode shapes do not show a significant difference, compared to the corresponding dry ones, but the location of maximum displacement shift slightly in the vertical direction. It must also be realized that for all the depth ratios, the wet mode shapes preserve their symmetry or antisymmetry with respect to the vertical axis passing through the longitudinal center of the plate.

16.3.2 Horizontal Cylindrical Shell Partially Filled with Fluid

In the second numerical example, the hydroelastic vibration analysis of a horizontal cylindrical shell partially filled with fluid is considered (see Fig. 16.9). The mechanical and geometrical properties of the cylindrical shell are: Young's modulus, $E = 206$ GPa, Poisson's ratio, $\nu = 0.3$, mass density, $\rho_s = 7680$ kg/m^3, thickness, $t = 1$ mm, length, $l = 0.664$ m, radius, $r = 0.175$ m. d denotes the filling depth of fluid, which has a density of $\rho_f = 1025$ kg/m^3.

The cylindrical shell is sealed with thin circular caps at both ends. These caps are resistant to radial loads, allowing for forces acting on their normal planes. Zhang et al (2001) has emphasized that the effect of these end caps on the hydroelastic vibration of circular shells is negligible. Therefore, in the numerical analysis, it is

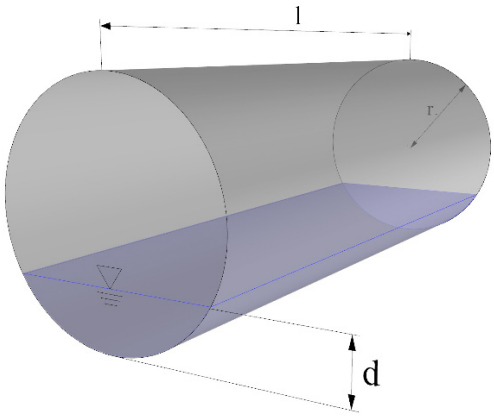

Fig. 16.9 Horizontal cylindrical shell partially filled with fluid.

assumed that the cylindrical shell is simply supported at both ends, instead of having caps at the ends.

Firstly, the in-vacuo dynamic response analysis of the cylindrical shell is carried out to obtain the in-vacuo natural frequencies and corresponding mode shapes, using the FEM formulation given in Appendix. To assess the accuracy of the obtained natural frequencies, a convergence study is carried out, and the results are compared with those obtained by ANSYS. In Table 16.4, the convergence of the first eight dry natural frequencies are presented for three different idealizations; 1900, 3470 and 7500 elements, respectively. As the number of elements increases, a monotonic convergence is observed, and the differences between the 3rd discretization and ANSYS become negligibly small. In Table 16.4, m denotes the number of half waves in the axial direction while n denotes the number of waves around the circumference.

Table 16.4 Convergence of dry natural frequencies (Hz).

Mode	This study			ANSYS
(m-n)	1900 El.	3470 El.	7500 El.	7500 El.
1-4	228.37	226.39	225.30	224.42
1-4	228.37	226.39	225.30	224.42
1-5	240.12	236.45	234.06	232.15
1-5	240.12	236.45	234.06	232.15
1-6	316.93	308.52	303.78	299.25
1-6	316.93	308.52	303.78	299.25
1-3	323.71	322.91	322.31	321.86
1-3	323.71	322.91	322.31	321.86

The calculated mode shapes for the first eight dry natural frequencies are shown in Fig. 16.10. As in Table 16.4 and Fig. 16.10, for each dry natural frequency, the mode shapes are obtained in pairs, satisfying the orthogonality condition. It must also be realized that the fundamental in-vacuo natural frequency does not correspond to the mode shape with the lowest number of waves around the circumference ($n = 2$). The order of modes depends on the internal strain energy and geometrical characteristics of the cylindrical shell under study.

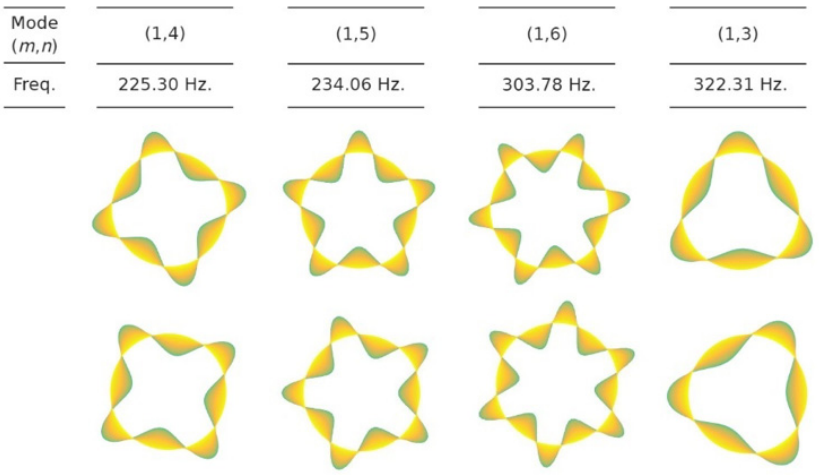

Fig. 16.10 First eight dry mode shapes of cylindrical shell.

In the second part of the analysis, the hydroelastic vibration characteristics of the cylindrical shell are investigated for three different filling depth-to-diameter ratios, $d/2r = 0.2, 0.5$ and 0.8. In ANSYS, the cylindrical shell is discretized with four-node quadrilateral SHELL181 elements, and fluid is modeled with FLUID30 elements (see Fig. 16.11).

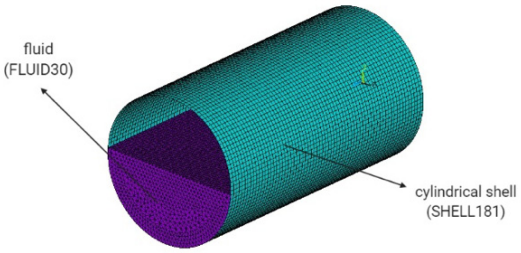

Fig. 16.11 ANSYS model of horizontal cylindrical shell partially filled with fluid ($d/2r = 0.50$).

Table 16.5 Convergence of wet natural frequencies (Hz) for filling ratios $d/2r = 0.20$, 0.50 and 0.80.

Mode	This study			ANSYS
	1350 El.	2195 El.	3190 El.	536400 El.
1	112.23	111.05	110.68	114.23
2	113.41	111.98	111.54	114.59
3	175.87	173.43	172.77	180.85
4	185.55	183.95	182.94	191.19
5	241.21	241.13	241.05	239.42
6	242.65	242.31	242.07	240.18

(a) $d/2r = 0.20$

Mode	This study			ANSYS
	952 El.	1710 El.	3752 El.	673400 El.
1	101.04	99.33	98.80	97.85
2	101.76	100.07	99.45	98.99
3	134.73	132.32	131.65	127.89
4	135.23	133.03	131.78	130.92
5	185.41	181.39	180.53	180.08
6	187.12	184.18	183.64	181.68

(b) $d/2r = 0.50$

Mode	This study			ANSYS
	1360 El.	2430 El.	1740 El.	968000 El.
1	97.47	96.01	95.58	94.02
2	97.96	96.45	96.02	94.92
3	115.21	113.13	112.47	110.04
4	116.96	115.09	114.34	113.08
5	141.30	139.21	138.46	136.38
6	148.16	145.20	144.77	143.53

(c) $d/2r = 0.80$

In order to check the convergence of the wet natural frequencies of cylindrical shell, for each filling ratio, three different idealizations are adopted, and the results are compared with those obtained by ANSYS. The number of hydrodynamic panels (boundary elements) over the wetted surface is 1350, 2195 and 3190 for $d/2r = 0.20$; 952, 1710 and 3752 for $d/2r = 0.50$; and 1360, 2430 and 5360 for $d/2r = 0.80$, respectively. As can be seen from Table 16.5, for all the filling ratios, results exhibit monotonic convergence, and the differences between the results of the 2nd and 3rd idealizations are negligibly small. Moreover, the predicted natural frequencies for the 3rd idealization compare very well with those obtained by ANSYS, and differences are in the range of 0.1% and 4.7%. As expected, the wet natural frequencies are lower than their in-vacuo counterparts, due to increasing inertia of the system, and the differences become significant with increasing filling ratio.

In Table 16.6, the generalized added mass coefficients for the first twelve distortional mode shapes are presented for filling ratios $d/2r = 0.20, 0.50$ and 0.80, respectively. These values are normalized to a generalized structural mass of 1 kgm^2. It is observed that the diagonal terms of the added mass matrices are considerably larger than the off-diagonal terms, which represent the hydrodynamic coupling between in-vacuo modes. Furthermore, the generalized added mass coefficients become larger for higher filling ratios due to increasing wetted surface area of the structure.

Table 16.6 Generalized added mass coefficients (kg m^2) for the horizontal cylindrical shell partially in contact with fluid.

m-n	1-4	1-4	1-5	1-5	1-6	1-6	1-3	1-3	1-7	1-7	1-8	1-8
1-4	1.40	0.03	-0.32	1.11	0.13	-0.70	-1.33	0.10	-0.21	0.02	-0.12	-0.01
1-4	0.03	1.46	-1.03	-0.32	0.61	0.13	0.10	1.38	0.02	-0.20	0.01	-0.12
1-5	-0.32	-1.03	1.20	0.01	-0.90	-0.01	0.03	-0.82	0.03	0.53	-0.01	-0.21
1-5	1.11	-0.32	0.01	1.26	0.01	-0.94	-0.79	-0.03	-0.51	0.02	0.20	-0.01
1-6	0.13	0.61	-0.90	0.01	0.97	0.00	-0.01	0.28	-0.02	-0.90	0.02	0.49
1-6	-0.70	0.13	-0.01	-0.94	0.00	0.96	0.31	0.01	0.87	-0.03	-0.45	0.02
1-3	-1.33	0.10	0.03	-0.79	-0.01	0.31	1.84	-0.02	-0.11	-0.03	0.24	0.00
1-3	0.10	1.38	-0.82	-0.03	0.28	0.01	-0.02	1.93	0.03	0.20	0.00	-0.30
1-7	-0.21	0.02	0.03	-0.51	-0.02	0.87	-0.11	0.03	0.81	0.01	-0.65	-0.03
1-7	0.02	-0.20	0.53	0.02	-0.90	-0.03	-0.03	0.20	0.01	0.85	0.03	-0.67
1-8	-0.12	0.01	-0.01	0.20	0.02	-0.45	0.24	0.00	-0.65	0.03	0.72	-0.01
1-8	-0.01	-0.12	-0.21	-0.01	0.49	0.02	0.00	-0.30	-0.03	-0.67	-0.01	0.69

(a) $d/2r = 0.20$

m-n	1-4	1-4	1-5	1-5	1-6	1-6	1-3	1-3	1-7	1-7	1-8	1-8
1-4	2.36	-0.05	-1.57	0.41	-0.20	0.01	-0.11	1.73	0.39	0.03	0.05	0.00
1-4	-0.05	2.50	-0.43	-1.55	-0.01	0.17	1.66	0.11	-0.03	0.36	0.00	-0.04
1-5	-1.57	-0.43	2.04	-0.03	-0.99	-0.33	-0.03	-0.23	0.08	0.01	-0.24	0.15
1-5	0.41	-1.55	-0.03	1.95	-0.35	-0.93	-0.25	0.03	-0.01	0.09	-0.17	-0.23
1-6	-0.20	-0.01	0.99	-0.35	1.64	0.04	-0.12	-0.36	1.06	-0.04	0.03	-0.09
1-6	0.01	0.17	-0.33	-0.93	0.04	1.68	-0.45	-0.09	-0.04	-0.99	-0.08	0.03
1-3	-0.11	1.66	-0.03	-0.25	-0.12	-0.45	2.85	0.03	-0.03	0.14	-0.28	-0.12
1-3	1.73	0.11	-0.23	0.03	0.36	-0.09	0.03	2.93	-0.09	0.03	-0.11	0.32
1-7	0.39	-0.03	0.08	-0.01	1.06	-0.04	-0.03	-0.09	1.41	0.03	0.17	-0.86
1-7	0.03	0.36	0.01	0.09	-0.04	-0.99	0.14	0.03	0.03	1.36	0.84	0.19
1-8	0.05	0.00	-0.24	-0.17	0.03	-0.08	-0.28	-0.11	0.17	0.84	1.20	0.03
1-8	0.00	-0.04	0.15	-0.23	-0.09	0.03	-0.12	0.32	-0.86	0.19	0.03	1.18

(b) $d/2r = 0.50$

m-n	1-4	1-4	1-5	1-5	1-6	1-6	1-3	1-3	1-7	1-7	1-8	1-8
1-4	3.55	0.00	-1.23	-0.03	-0.02	-0.70	-1.51	-0.03	0.00	-0.14	-0.23	-0.01
1-4	0.00	3.40	0.03	-1.22	-0.67	0.02	0.03	-1.60	-0.14	0.00	-0.01	0.24
1-5	-1.23	0.03	2.75	0.00	-0.02	-1.01	-0.71	-0.01	-0.01	-0.51	0.09	0.01
1-5	-0.03	-1.22	0.00	2.90	-0.96	0.02	0.01	-0.74	-0.51	0.01	0.01	-0.11
1-6	-0.02	-0.58	-0.02	-0.96	2.37	0.00	0.00	-0.09	-0.83	0.00	0.02	-0.47
1-6	-0.70	0.02	-1.01	0.02	0.00	2.37	-0.11	0.00	0.00	-0.78	0.44	0.02
1-3	-1.51	0.07	-0.71	0.01	0.00	-0.11	4.50	0.01	0.00	0.22	-0.28	-0.01
1-3	-0.03	-1.61	-0.01	-0.74	-0.09	0.00	0.01	4.25	0.26	0.00	-0.01	0.31
1-7	0.00	-0.04	-0.01	-0.51	-0.83	0.00	0.00	0.26	1.96	0.00	0.03	-0.70
1-7	-0.14	0.00	-0.51	0.01	0.00	-0.78	0.22	0.00	0.00	2.03	0.67	0.03
1-8	-0.23	-0.02	0.09	0.01	0.02	0.44	-0.28	-0.01	0.03	0.67	1.69	0.00
1-8	-0.01	0.24	0.01	-0.11	-0.47	0.02	-0.01	0.31	-0.70	0.03	0.00	1.72

(c) $d/2r = 0.80$

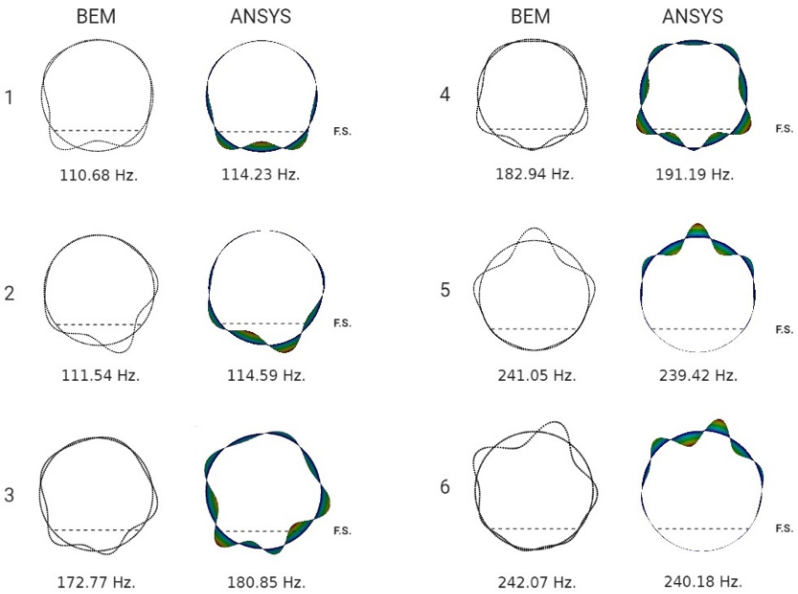

Fig. 16.12 Natural frequencies and associated mode shapes of cylindrical shell for $d/2r = 0.20$.

The first six wet natural frequencies and associated mode shapes are shown in Figs. 16.12, 16.13 and 16.14, for $d/2r = 0.20, 0.50$ and 0.80, respectively. All the wet modes shown have one longitudinal half wave ($m = 1$) along the longitudinal axis, and only the circumferential mode shapes are presented. In contrast to mode shapes under in-vacuo condition, the wet mode shapes do not occur in pairs, and they are simply numbered with increasing frequency. For all the filling ratios, mode shapes are either symmetric or antisymmetric, with respect to the axis passing through the center of the cylinder and perpendicular to the free surface. In general, the predicted mode shapes compare very well with those obtained by ANSYS.

16.4 Conclusions

In this study, a FE-BE method is presented for the hydroelastic vibration analysis of plates and shells partially contact with fluid. In order to show the applicability of the method, two different numerical examples-a vertical rectangular plate in contact with fluid on one side and a horizontal cylindrical shell partially filled with fluid-are studied. The predicted results by the present method are also compared with those obtained by ANSYS-a commercial software. It can be concluded that the presented numerical procedure is suitable to investigate relatively high-frequency vibrations of elastic structures partially in contact with fluid.

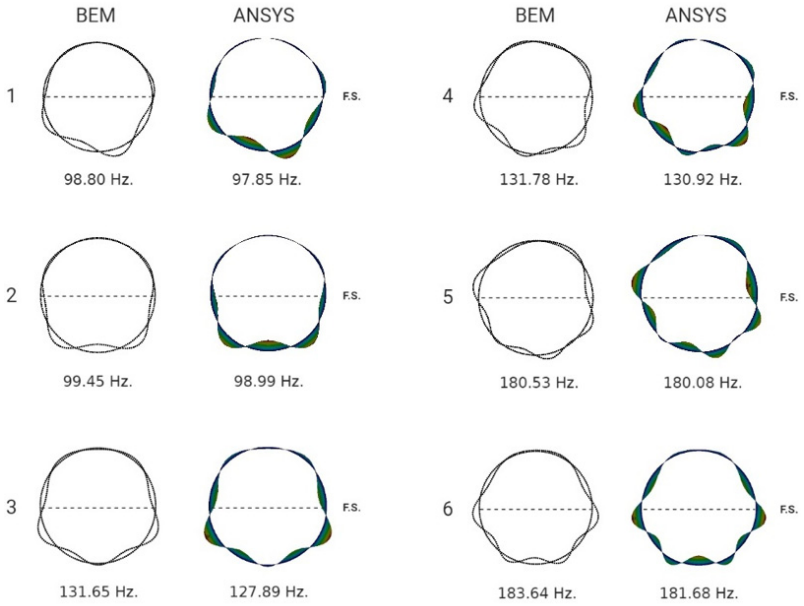

Fig. 16.13 Natural frequencies and associated mode shapes of cylindrical shell for $d/2r = 0.50$.

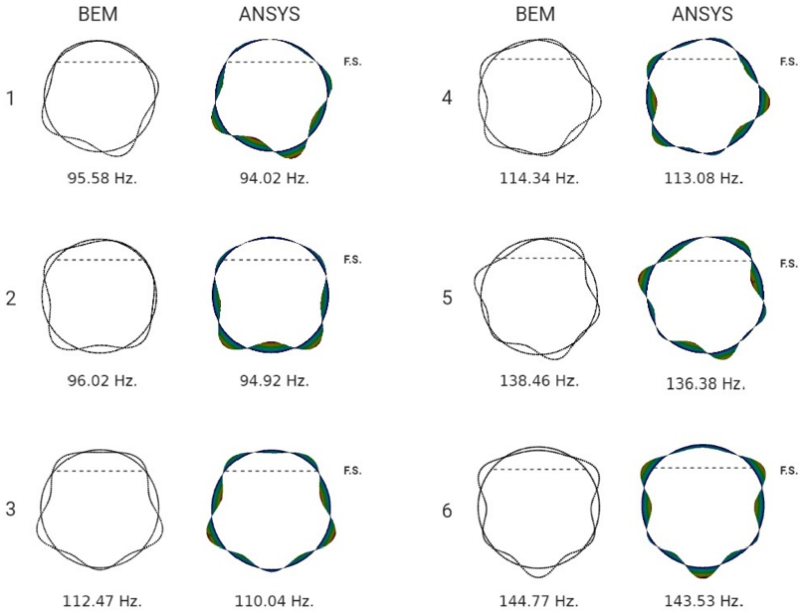

Fig. 16.14 Natural frequencies and associated mode shapes of cylindrical shell for $d/2r = 0.80$.

In the numerical examples, idealizations in both in-vacuo and wet analyses are independent from each other, and both depend on the complexity of the structure and the convergence. For both the rectangular plate and the horizontal cylindrical shell, the convergence studies (see Tables 16.1, 16.2, 16.4 and 16.5) show that differences are in an acceptable range. Also, the predicted frequencies compare very well with the results obtained by ANSYS.

The present work demonstrates the versatility of the proposed method by studying two different structures partially in contact with fluid. Moreover, the numerical framework can be adopted to analyze more complex structures such as materials exhibiting higher-gradient effects (for example, see those presented in dell'Isola and Seppecher, 1995; Alibert et al, 2003; dell'Isola et al, 2012; Cuomo et al, 2016; Abali et al, 2017; Barchiesi et al, 2019; Vangelatos et al, 2019c,b,a; dell'Isola et al, 2019a,b; Eremeyev et al, 2018; Rahali et al, 2020; Eremeyev and Turco, 2020; Chróścielewski et al, 2020). Application of the presented framework for such complex materials is currently under investigation by the authors. Also, the free surface effects should be taken into account to have a better understanding of the phenomenon.

Appendix

In this study, flat shell elements are used to conduct the in-vacuo analyses. In the formulation of this shell element, it is assumed that bending and in-plane force resultants are independent from each other. Therefore, the problem is considered as a combination of 2-D plane stress and plate bending problems. Then, element stiffness and mass matrices of each problem are combined in a suitable manner to define total element stiffness and mass matrices. In this study, the plane stress problem is formulated with bilinear displacement rectangular elements, and the plate bending problem is modeled with MZC (Melosh-Zienkiewicz-Cheung) rectangular element formulation (see Fig. 16.15).

Plane Stress Formulation

There is a wide number of elements developed based upon the assumptions of two-dimensional elasticity. Among the formulations available, the bilinear displacement rectangle element, developed by Melosh (1963) is preferred in this study to model plane stress field of flat shell elements. A geometric configuration of this type of element with a thickness t is given in Fig. 16.15. The dimensionless centroidal coordinates are defined as follows

$$\xi = \frac{x}{a}, \qquad \eta = \frac{y}{b} \tag{16.23}$$

where $2a$ and $2b$ are width and height, respectively. For plane stress elements, the displacement field is defined with translations in the plane, formed by local x and y

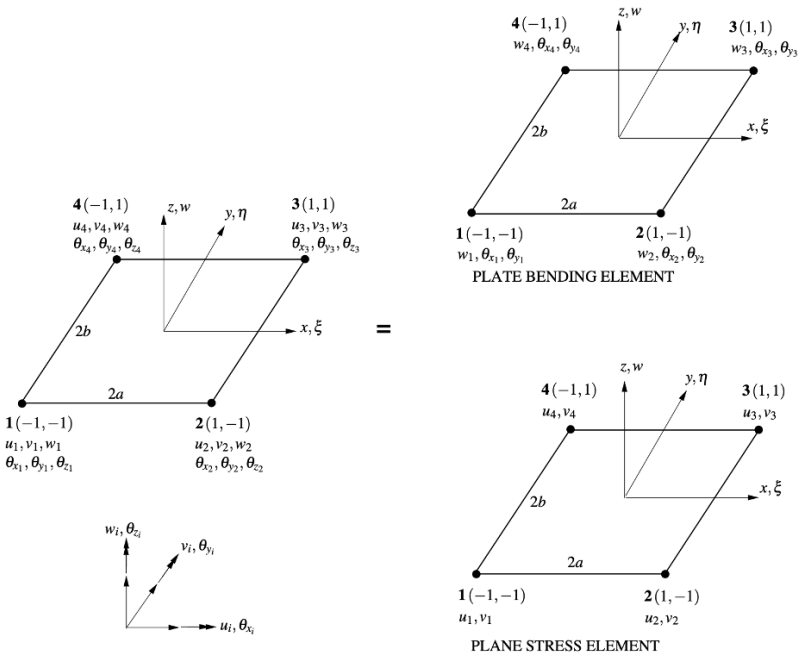

Fig. 16.15 Flat shell element.

coordinates. The first node is placed lower left corner, and the consecutive nodes are designated in counterclockwise direction. The nodal displacement vector is written as

$$\mathbf{q} = \{q_1, q_2, ..., q_7, q_8\} = \{u_1, v_1, ..., u_4, v_4\}. \tag{16.24}$$

For the displacement field, which is bilinear in ξ and η, the displacements are defined as

$$u = c_1 + c_2\xi + c_3\eta + c_4\xi\eta, \tag{16.25}$$

$$v = c_5 + c_6\xi + c_7\eta + c_8\xi\eta. \tag{16.26}$$

By using these displacement functions, the geometric matrix, $\mathbf{G}$, is introduced as follows:

$$\mathbf{G} = \begin{bmatrix} 1\ \xi\ \eta\ \xi\eta\ 0\ 0\ 0\ \ 0 \\ 0\ 0\ 0\ \ 0\ \ 1\ \xi\ \eta\ \xi\eta \end{bmatrix} \tag{16.27}$$

The geometric matrix is evaluated at each node to obtain the following matrix:

$$\mathbf{H} = \begin{bmatrix} \mathbf{g}_1 \\ \mathbf{g}_2 \\ \mathbf{g}_3 \\ \mathbf{g}_4 \end{bmatrix} = \begin{bmatrix} 1 & -1 & -1 & 1 & 0 & 0 & 0 & 0 \\ 0 & 0 & 0 & 0 & 1 & -1 & -1 & 1 \\ 1 & 1 & -1 & -1 & 0 & 0 & 0 & 0 \\ 0 & 0 & 0 & 0 & 1 & 1 & -1 & -1 \\ 1 & 1 & 1 & 1 & 0 & 0 & 0 & 0 \\ 0 & 0 & 0 & 0 & 1 & 1 & 1 & 1 \\ 1 & -1 & 1 & -1 & 0 & 0 & 0 & 0 \\ 0 & 0 & 0 & 0 & 1 & -1 & 1 & -1 \end{bmatrix} \tag{16.28}$$

where $\mathbf{g}_i$ is a 2×8 matrix evaluated at ith node ($i = 1, 2, 3, 4$). Then, the matrix formed by displacement shape functions, $\mathbf{N} = \mathbf{G}\mathbf{H}^{-1}$, is written as:

$$\mathbf{N} = \begin{bmatrix} N_1 & 0 & N_2 & 0 & N_3 & 0 & N_4 & 0 \\ 0 & N_1 & 0 & N_2 & 0 & N_3 & 0 & N_4 \end{bmatrix} \tag{16.29}$$

where

$$N_1 = \frac{1}{4}(1-\xi)(1-\eta), \qquad N_2 = \frac{1}{4}(1+\xi)(1-\eta),$$
$$N_3 = \frac{1}{4}(1+\xi)(1+\eta), \qquad N_4 = \frac{1}{4}(1-\xi)(1+\eta).$$

Next, in order to define the linear differential operator formed by the derivatives with respect to cartesian coordinates, chain rule is applied as follows:

$$\frac{\partial}{\partial x} = \frac{\partial}{\partial \xi}\frac{\partial \xi}{\partial x} + \frac{\partial}{\partial \eta}\frac{\partial \eta}{\partial x} = \frac{1}{a}\frac{\partial}{\partial \xi},$$
$$\frac{\partial}{\partial y} = \frac{\partial}{\partial \xi}\frac{\partial \xi}{\partial y} + \frac{\partial}{\partial \eta}\frac{\partial \eta}{\partial y} = \frac{1}{b}\frac{\partial}{\partial \eta}.$$

Then, the differential operator, $\mathbf{D}^p$, is written as:

$$\mathbf{D}^p = \begin{bmatrix} \frac{\partial}{\partial x} & 0 \\ 0 & \frac{\partial}{\partial y} \\ \frac{\partial}{\partial y} & \frac{\partial}{\partial x} \end{bmatrix} = \begin{bmatrix} \frac{1}{a}\frac{\partial}{\partial \xi} & 0 \\ 0 & \frac{1}{b}\frac{\partial}{\partial \eta} \\ \frac{1}{b}\frac{\partial}{\partial \eta} & \frac{1}{a}\frac{\partial}{\partial \xi} \end{bmatrix}. \tag{16.30}$$

For isotropic materials, the stress-strain operator is defined as follows:

$$\mathbf{E} = \frac{E}{(1-\nu^2)} \begin{bmatrix} 1 & \nu & 0 \\ \nu & 1 & 0 \\ 0 & 0 & \frac{1-\nu}{2} \end{bmatrix} \tag{16.31}$$

where E and ν represent Young's modulus and Poisson's ratio, respectively. Finally, element stiffness matrix, $\mathbf{K}$, and mass matrix, $\mathbf{M}$, are calculated as follows:

$$\mathbf{K}^p = abt \int_{-1}^{+1}\int_{-1}^{+1} \mathbf{B}^T \mathbf{E} \mathbf{B}\, d\xi d\eta \tag{16.32}$$

$$\mathbf{M}^p = \rho abt \int_{-1}^{+1}\int_{-1}^{+1} \mathbf{G}^T \mathbf{G}\, d\xi d\eta \tag{16.33}$$

In the expressions given in Eqs. 16.32 and 16.33, the matrix $\mathbf{B}$ is defined as

$$\mathbf{B} = \mathbf{D}\mathbf{G} = \frac{1}{ab} \begin{bmatrix} 0 & b & 0 & b\eta & 0 & 0 & 0 & 0 \\ 0 & 0 & 0 & 0 & 0 & 0 & a & a\xi \\ 0 & 0 & a & a\xi & 0 & b & 0 & b\eta \end{bmatrix}. \tag{16.34}$$

The element stiffness and mass matrices given in Eqs. 16.32 and 16.33 have a dimension of 8×8. To combine these matrices with those of the plate bending problem, it is convenient to divide these matrices as follows:

$$\mathbf{K}^p = \begin{bmatrix} \left[\mathbf{K}^p_{11}\right] & & & \\ \left[\mathbf{K}^p_{21}\right] & \left[\mathbf{K}^p_{22}\right] & & \text{Sym.} \\ \left[\mathbf{K}^p_{31}\right] & \left[\mathbf{K}^p_{32}\right] & \left[\mathbf{K}^p_{33}\right] & \\ \left[\mathbf{K}^p_{41}\right] & \left[\mathbf{K}^p_{42}\right] & \left[\mathbf{K}^p_{43}\right] & \left[\mathbf{K}^p_{44}\right] \end{bmatrix}_{8\times 8}, \tag{16.35}$$

$$\mathbf{M}^p = \begin{bmatrix} \left[\mathbf{M}^p_{11}\right] & & & \\ \left[\mathbf{M}^p_{21}\right] & \left[\mathbf{M}^p_{22}\right] & & \text{Sym.} \\ \left[\mathbf{M}^p_{31}\right] & \left[\mathbf{M}^p_{32}\right] & \left[\mathbf{M}^p_{33}\right] & \\ \left[\mathbf{M}^p_{41}\right] & \left[\mathbf{M}^p_{42}\right] & \left[\mathbf{M}^p_{43}\right] & \left[\mathbf{M}^p_{44}\right] \end{bmatrix}_{8\times 8}, \tag{16.36}$$

where $\left[\mathbf{K}^p_{ij}\right]$ and $\left[\mathbf{M}^p_{ij}\right]$ are 2×2 sub-matrices of the element stiffness and mass matrices, respectively $(i, j = 1, 2, 3, 4)$. The superscript p denotes the in-plane effects.

Plate Bending Formulation

In this study, MZC rectangular element, originally developed by Melosh Melosh (1963), is used to model plate bending contributions of flat shell elements. As seen from Fig. 16.15, this element has only one generic displacement, w, and rotations,

θ_{x_i} and θ_{y_i}, with respect to the local axes x and y. For this type of plate element, the following nodal displacement vector is introduced

$$\mathbf{q} = \{q_1, q_2, ..., q_{12}\} = \{w_1, \theta_{x_1}, \theta_{y_1}, ..., w_4, \theta_{x_4}, \theta_{y_4}\} \tag{16.37}$$

and the displacement function is expressed as

$$\begin{aligned} w = {} & c_1 + c_2\xi + c_3\eta + c_4\xi^2 + c_5\xi\eta + c_6\eta^2 \\ & + c_7\xi^3 + c_8\xi^2\eta + c_9\xi\eta^2 + c_{10}\eta^3 + c_{11}\xi^3\eta + c_{12}\xi\eta^3. \end{aligned} \tag{16.38}$$

The matrix formed by displacement shape functions is derived as

$$\mathbf{N}_i = [N_{i_1} N_{i_2} N_{i_3}]$$

where

$$\begin{aligned} N_{i_1} &= \frac{1}{8}(1+\xi_0)(1+\eta_0)(2+\xi_0+\eta_0-\xi^2-\eta^2) \\ N_{i_2} &= \frac{-1}{8}\eta_i(1+\xi_0)(1-\eta_0)(1+\eta_0)^2 \\ N_{i_3} &= \frac{1}{8}\xi_i(1-\xi_0)(1+\eta_0)(1+\xi_0)^2 \end{aligned}$$

and

$$\xi_0 = \xi_i\xi, \qquad \eta_0 = \eta_i\eta, \qquad (i = 1, 2, 3, 4)$$

The differential operator (curvature matrix) for the plate bending problem is defined as follows:

$$\mathbf{D}^b = \{\frac{\partial^2}{\partial x^2}, \frac{\partial^2}{\partial y^2}, \frac{2\partial^2}{\partial x \partial y}\}. \tag{16.39}$$

By utilizing the curvature matrix and shape functions, one can obtain strain-displacement matrix as follows

$$\mathbf{B}_i^b = \mathbf{D}^b\mathbf{N}_i = \begin{bmatrix} N_{i_{1,xx}} & N_{i_{2,xx}} & N_{i_{3,xx}} \\ N_{i_{1,yy}} & N_{i_{2,yy}} & N_{i_{3,yy}} \\ 2N_{i_{1,xy}} & 2N_{i_{2,xy}} & 2N_{i_{3,xy}} \end{bmatrix} \qquad (i = 1, 2, 3, 4), \tag{16.40}$$

The local strain-displacement matrix is a 3×12 matrix, and it is formed as

$$\mathbf{B}^b = \begin{bmatrix} \mathbf{B}_1^b & \mathbf{B}_2^b & \mathbf{B}_3^b & \mathbf{B}_4^b \end{bmatrix}_{3\times 12} \tag{16.41}$$

In particular, $\mathbf{B}_1^b$ is calculated as

$$\mathbf{B}_1^b = \frac{1}{4a^2b^2}\begin{bmatrix} 3\xi(1-\eta)b^2 & 0 & (1-3\xi)(1-\eta)ab^2 \\ 3(1-\xi)\eta a^2 & -(1-\xi)(1-3\eta)a^2b & 0 \\ (4-3\xi^2-3\eta^2)ab & (1-\eta)(1+3\eta)ab^2 & -(1-\xi)(1+3\xi)a^2b \end{bmatrix} \tag{16.42}$$

For an isotropic and homogeneous material, the generalized bending constitutive matrix is given as

$$\mathbf{E}^b = \frac{Et^3}{12(1-\nu^2)}\begin{bmatrix} 1 & \nu & 0 \\ \nu & 1 & 0 \\ 0 & 0 & \frac{1}{2}(1-\nu) \end{bmatrix}. \tag{16.43}$$

Finally, the element sitffness matrix, $\mathbf{K}^b$, and the mass matrix, $\mathbf{M}^b$, for plate bending elements are calculated as follows

$$\mathbf{K}^b = ab\int_{-1}^{1}\int_{-1}^{1} \mathbf{B}^{b^T}\mathbf{E}^b\mathbf{B}^b\, d\xi\, d\eta, \tag{16.44}$$

$$\mathbf{M}^b = \rho tab\int_{-1}^{1}\int_{-1}^{1} \mathbf{N}^T\mathbf{N}\, d\xi\, d\eta. \tag{16.45}$$

The element stiffness and mass matrices of bending element given in Eqs. 16.44 and 16.45 have dimensions of 12×12. Again, for convenience, these matrices are divided into sub-matrices to show the contributions to each degree of freedom as follows

$$\mathbf{K}^b = \begin{bmatrix} \left[\mathbf{K}_{11}^b\right] & & & \\ \left[\mathbf{K}_{21}^b\right] & \left[\mathbf{K}_{22}^b\right] & & \text{Sym.} \\ \left[\mathbf{K}_{31}^b\right] & \left[\mathbf{K}_{32}^b\right] & \left[\mathbf{K}_{33}^b\right] & \\ \left[\mathbf{K}_{41}^b\right] & \left[\mathbf{K}_{42}^b\right] & \left[\mathbf{K}_{43}^b\right] & \left[\mathbf{K}_{44}^b\right] \end{bmatrix}_{12\times 12} \tag{16.46}$$

$$\mathbf{M}^b = \begin{bmatrix} \left[\mathbf{M}_{11}^b\right] & & & \\ \left[\mathbf{M}_{21}^b\right] & \left[\mathbf{M}_{22}^b\right] & & \text{Sym.} \\ \left[\mathbf{M}_{31}^b\right] & \left[\mathbf{M}_{32}^b\right] & \left[\mathbf{M}_{33}^b\right] & \\ \left[\mathbf{M}_{41}^b\right] & \left[\mathbf{M}_{42}^b\right] & \left[\mathbf{M}_{43}^b\right] & \left[\mathbf{M}_{44}^b\right] \end{bmatrix}_{12\times 12} \tag{16.47}$$

where $\left[\mathbf{K}_{ij}^{b}\right]$ and $\left[\mathbf{M}_{ij}^{b}\right]$ are 2×2 sub-matrices of the element stiffness and mass matrices, respectively $(i, j = 1, 2, 3, 4)$. The superscript b denotes the bending effects.

Derivation of Combined Stiffness and Mass Matrices of Flat Shell Element

As mentioned before, in-plane and bending counterparts of the mass and stiffness matrices are combined to get the total stiffness and mass matrices in local coordinate system. The total stiffness matrix is given as follows

$$\mathbf{K} = \begin{bmatrix}
\mathbf{K}_{11}^{p} & & & & & & & & & & & & & & & & & & & & & & & \\
0\ 0 & & & & & & & & & & & & & & & & & & & & & & & \\
0\ 0 & \mathbf{K}_{11}^{b} & & & & & & & & & & & & & & & & & & & & & & \\
0\ 0 & & & & & & & & & & & & & & & & & & & & & & & \\
0\ 0 & 0\ 0\ 0\ 0 & 0 & & & & & & & & & & & & & & & & & & & & & \\
\mathbf{K}_{21}^{p} & \begin{matrix}0\ 0\ 0\ 0\\0\ 0\ 0\ 0\end{matrix} & \mathbf{K}_{22}^{p} & & & & & & & & & & & & & & & & & & & & & \\
0\ 0 & & 0 & 0\ 0 & & & & & & & & & & & & & & & & & & & & \\
0\ 0 & \mathbf{K}_{21}^{b} & 0 & 0\ 0 & \mathbf{K}_{22}^{b} & & & & & & & & & & & & & & & & & & & \\
0\ 0 & & 0 & 0\ 0 & & & & & & & & & & & & & & & & & & & & \\
0\ 0 & 0\ 0\ 0\ 0 & 0 & 0\ 0 & 0\ 0\ 0\ 0 & & & & & & & & & & & & & & & & & & & \\
\mathbf{K}_{31}^{p} & \begin{matrix}0\ 0\ 0\ 0\\0\ 0\ 0\ 0\end{matrix} & \mathbf{K}_{32}^{p} & \begin{matrix}0\ 0\ 0\ 0\\0\ 0\ 0\ 0\end{matrix} & \mathbf{K}_{33}^{p} & & & & & & & & & & & & & & & & & & \\
0\ 0 & & 0 & 0\ 0 & & 0 & 0\ 0 & & & & & & & & & & & & & & & & \\
0\ 0 & \mathbf{K}_{31}^{b} & 0 & 0\ 0 & \mathbf{K}_{32}^{b} & 0 & 0\ 0 & \mathbf{K}_{33}^{p} & & & & & & & & & & & & & & & \\
0\ 0 & & 0 & 0\ 0 & & 0 & 0\ 0 & & & & & & & & & & & & & & & & \\
0\ 0 & 0\ 0\ 0\ 0 & 0 & 0\ 0 & 0\ 0\ 0\ 0 & 0 & 0\ 0 & 0\ 0\ 0\ 0 & & & & & & & & & & & & & & \\
\mathbf{K}_{41}^{p} & \begin{matrix}0\ 0\ 0\ 0\\0\ 0\ 0\ 0\end{matrix} & \mathbf{K}_{42}^{p} & \begin{matrix}0\ 0\ 0\ 0\\0\ 0\ 0\ 0\end{matrix} & \mathbf{K}_{43}^{p} & \begin{matrix}0\ 0\ 0\ 0\\0\ 0\ 0\ 0\end{matrix} & \mathbf{K}_{44}^{p} & & & & & & & & & & & & & & & \\
0\ 0 & & 0 & 0\ 0 & & 0 & 0\ 0 & & 0 & 0\ 0 & & & & & & & & & & & & & \\
0\ 0 & \mathbf{K}_{41}^{b} & 0 & 0\ 0 & \mathbf{K}_{42}^{b} & 0 & 0\ 0 & \mathbf{K}_{43}^{p} & 0 & 0\ 0 & \mathbf{K}_{44}^{b} & & & & & & & & & & & & \\
0\ 0 & & 0 & 0\ 0 & & 0 & 0\ 0 & & 0 & 0\ 0 & & & & & & & & & & & & & \\
0\ 0 & 0\ 0\ 0\ 0 & 0 & 0\ 0 & 0\ 0\ 0\ 0 & 0 & 0\ 0 & 0\ 0\ 0\ 0 & 0 & 0\ 0 & 0\ 0\ 0\ 0 & & & & & & & & & & & \\
\end{bmatrix}_{24\times 24} \tag{16.48}$$

In a similar manner, the mass matrix, $\mathbf{M}$ can be obtained. There are two important points to emphasize here. First, as can be seen from Eq. (16.48), the displacements resulting from in-plane forces have no effect on bending deformations, and vice versa. Second, the rotational deformation, θ_{z_i} is not included in the problem.

The derived mass and stiffness matrices in the local coordinates must be transformed into an identified reference coordinate system. All the transformations are accomplished by a simple process. The displacements of a node are transformed from global to local coordinates by the following transformation matrix

$$\mathbf{T} = \begin{bmatrix} \Lambda & 0 & 0 & 0 & 0 & 0 \\ 0 & \Lambda & 0 & 0 & 0 & 0 \\ 0 & 0 & \Lambda & 0 & 0 & 0 \\ 0 & 0 & 0 & \Lambda & 0 & 0 \\ 0 & 0 & 0 & 0 & \Lambda & 0 \\ 0 & 0 & 0 & 0 & 0 & \Lambda \end{bmatrix} \tag{16.49}$$

with Λ being a 3×3 matrix of direction cosines between the two sets of axes given by

$$\Lambda = \begin{bmatrix} \cos(\xi, x) & \cos(\xi, \eta) & \cos(\xi, z) \\ \cos(\eta, x) & \cos(\eta, \eta) & \cos(\eta, z) \\ \cos(\zeta, x) & \cos(\zeta, \eta) & \cos(\zeta, z) \end{bmatrix} \tag{16.50}$$

where $\cos(\xi, x)$ is the cosine of the angle between ξ and x axes. Thus, the stiffness and mass matrices of an element in global coordinates are computed with the following transformation

$$\bar{\mathbf{K}} = \mathbf{T}^T \mathbf{K}\, \mathbf{T}, \tag{16.51}$$

$$\bar{\mathbf{M}} = \mathbf{T}^T \mathbf{M}\, \mathbf{T} \tag{16.52}$$

where $\bar{\mathbf{K}}$ and $\bar{\mathbf{M}}$ are the global stiffness and mass matrices. Once the stiffness matrices of all the elements have been determined in a common global coordinate system, the assembly of the elements follow the standard solution pattern.

References

ANSYS (2013) Mechanical APDL Command Reference, ANSYS, Inc., Release 15.0

Abali BE, Müller WH, dell'Isola F (2017) Theory and computation of higher gradient elasticity theories based on action principles. Archive of Applied Mechanics 87(9):1495–1510

Abd-alla AN, Alshaikh F, Del Vescovo D, Spagnuolo M (2017) Plane waves and eigenfrequency study in a transversely isotropic magneto-thermoelastic medium under the effect of a constant angular velocity. Journal of Thermal Stresses 40(9):1079–1092

Alessandroni S, Andreaus U, dell'Isola F, Porfiri M (2005) A passive electric controller for multimodal vibrations of thin plates. Computers & structures 83(15-16):1236–1250

Alibert JJ, Seppecher P, dell'Isola F (2003) Truss modular beams with deformation energy depending on higher displacement gradients. Mathematics and Mechanics of Solids 8(1):51–73

Amabili M, Dalpiaz G (1995) Breathing vibrations of a horizontal circular cylindrical tank shell, partially filled with liquid. Journal of vibration and acoustics 117(2):187–191

Amabili M, Frosali G, Kwak MK (1996) Free vibrations of annular plates coupled with fluids. Journal of sound and vibration 191(5):825–846

Askari E, Jeong KH (2010) Hydroelastic vibration of a cantilever cylindrical shell partially submerged in a liquid. Ocean Engineering 37(11-12):1027–1035

Askari E, Jeong KH, Amabili M (2013) Hydroelastic vibration of circular plates immersed in a liquid-filled container with free surface. Journal of sound and vibration 332(12):3064–3085

Barchiesi E, Laudato M, Di Cosmo F (2018) Wave dispersion in non-linear pantographic beams. Mechanics Research Communications 94:128–132

Barchiesi E, Spagnuolo M, Placidi L (2019) Mechanical metamaterials: a state of the art. Mathematics and Mechanics of Solids 24(1):212–234

Baroudi D, Giorgio I, Battista A, Turco E, Igumnov LA (2019) Nonlinear dynamics of uniformly loaded elastica: Experimental and numerical evidence of motion around curled stable equilibrium configurations. ZAMM-Journal of Applied Mathematics and Mechanics/Zeitschrift für Angewandte Mathematik und Mechanik p e201800121

Bersani AM, Della Corte A, Piccardo G, Rizzi NL (2016) An explicit solution for the dynamics of a taut string of finite length carrying a traveling mass: the subsonic case. Zeitschrift für angewandte Mathematik und Physik 67(4):108

Bishop RED, Price W (1979) Hydroelasticity of Ships. Cambridge University Press

Cazzani A, Rizzi NL, Stochino F, Turco E (2018) Modal analysis of laminates by a mixed assumed-strain finite element model. Mathematics and Mechanics of Solids 23(1):99–119

Chiba M, Yamaki N, Tani J (1984a) Free vibration of a clamped-free circular cylindrical shell partially filled with liquid–Part I: Theoretical analysis. Thin-walled structures 2(3):265–284

Chiba M, Yamaki N, Tani J (1984b) Free vibration of a clamped-free circular cylindrical shell partially filled with liquid–Part II: Numerical results. Thin-Walled Structures 2(4):307–324

Cho DS, Kim BH, Vladimir N, Choi TM (2014) Natural vibration analysis of vertical rectangular plates and stiffened panels in contact with fluid on one side. Proceedings of the Institution of Mechanical Engineers, Part M: Journal of Engineering for the Maritime Environment 230(1):114–125

Chróścielewski J, dell'Isola F, Eremeyev VA, Agnieszka S (2020) On rotational instability within the nonlinear six-parameter shell theory. International Journal of Solids and Structures, doi: 10.1016/j.ijsolstr.2020.04.030

Cuomo M, dell'Isola F, Greco L (2016) Simplified analysis of a generalized bias test for fabrics with two families of inextensible fibres. Zeitschrift für angewandte Mathematik und Physik 67(3):61

Datta N, Jindal R (2019) Modelling a spade rudder as a hollow two-way tapered kirchhoff's plate: free dry and wet vibration study with numerical verification. Applied Ocean Research 82:385–396

De Espinosa FM, Gallego-Juarez JA (1984) On the resonance frequencies of water-loaded circular plates. Journal of sound and vibration 94(2):217–222

dell'Isola F, Seppecher P (1995) The relationship between edge contact forces, double forces and interstitial working allowed by the principle of virtual power. Comptes rendus de l'Académie des sciences Série IIb, Mécanique, physique, astronomie p 7

dell'Isola F, Seppecher P, Madeo A (2012) How contact interactions may depend on the shape of Cauchy cuts in Nth gradient continua: approach "à la D'alembert". Zeitschrift für angewandte Mathematik und Physik 63(6):1119–1141

dell'Isola F, Seppecher P, Alibert JJ, et al (2019a) Pantographic metamaterials: an example of mathematically driven design and of its technological challenges. Continuum Mechanics and Thermodynamics 31(4):851–884

dell'Isola F, Seppecher P, Spagnuolo M, et al (2019b) Advances in pantographic structures: design, manufacturing, models, experiments and image analyses. Continuum Mechanics and Thermodynamics 31(4):1231–1282

Eremeyev VA, Turco E (2020) Enriched buckling for beam-lattice metamaterials. Mechanics Research Communications 103:103,458

Eremeyev VA, dell'Isola F, Boutin C, Steigmann D (2018) Linear pantographic sheets: existence and uniqueness of weak solutions. Journal of Elasticity 132(2):175–196

Ergin A, Temarel P (2002) Free vibration of a partially liquid-filled and submerged, horizontal cylindrical shell. Journal of Sound and vibration 254(5):951–965

Ergin A, Uğurlu B (2003) Linear vibration analysis of cantilever plates partially submerged in fluid. Journal of Fluids and Structures 17(7):927–939

Fu Y, Price WG (1987) Interactions between a partially or totally immersed vibrating cantilever plate and the surrounding fluid. Journal of Sound and Vibration 118(3):495–513

Giorgio I, Del Vescovo D (2018) Non-linear lumped-parameter modeling of planar multi-link manipulators with highly flexible arms. Robotics 7(4):60

Giorgio I, Del Vescovo D (2019) Energy-based trajectory tracking and vibration control for multilink highly flexible manipulators. Mathematics and Mechanics of Complex Systems 7(2):159–174

Giorgio I, Rizzi NL, Turco E (2017) Continuum modelling of pantographic sheets for out-of-plane bifurcation and vibrational analysis. Proceedings of the Royal Society A: Mathematical, Physical and Engineering Sciences 473(2207):20170,636

Goncalves PB, Ramos NRSS (1996) Free vibration analysis of cylindrical tanks partially filled with liquid. Journal of Sound and Vibration 195(3):429–444

Hsu CY, Jen CY (2010) The transient response of imperfect thin-walled stiffened cylindrical shell exposed to side-on underwater explosion. In: ASME 2009 28th International Conference on Ocean, Offshore and Arctic Engineering, American Society of Mechanical Engineers Digital Collection, pp 11–21

Jeong KH (1999) Dynamics of a concentrically or eccentrically submerged circular cylindrical shell in a fluid-filled container. Journal of Sound and vibration 224(4):709–732

Jeong KH (2003) Free vibration of two identical circular plates coupled with bounded fluid. Journal of Sound and Vibration 260(4):653–670

Jeong KH, Kim JW (2009) Hydroelastic vibration analysis of two flexible rectangular plates partially coupled with a liquid. Nuclear Engineering and Technology 41(3):335–346

Jeong KH, Lee SC (1996) Fourier series expansion method for free vibration analysis of either a partially liquid-filled or a partially liquid-surrounded circular cylindrical shell. Computers & structures 58(5):937–946

Junge M, Brunner D, Gaul L (2011) Solution of fe-be coupled eigenvalue problems for the prediction of the vibro-acoustic behavior of ship-like structures. International Journal for Numerical Methods in Engineering 87(7):664–676

Kalinowski AJ (1974) Fluid-structure interaction problems using finite elements. In: Fifth Navy-NASTRAN Colloquim, Naval Ship Research adn Development Center, Bethesda, Maryland, pp 71–86

Kito F (1970) Principles of Hydro-elasticity. Keio University

Kwak MK (1991) Vibration of circular plates in contact with water. Journal of Applied Mechanics 58(2):480–483

Kwak MK (1997) Hydroelastic vibration of circular plates. Journal of Sound and Vibration 201(3):293–303

Kwak MK, Yang DH (2013) Free vibration analysis of cantilever plate partially submerged into a fluid. Journal of Fluids and Structures 40:25–41

Liang CC, Hsu CY, Lai WH (2001) A study of transient responses of a submerged spherical shell under shock waves. Ocean engineering 28(1):71–94

Liao CY, Ma CC (2016) Vibration characteristics of rectangular plate in compressible inviscid fluid. Journal of Sound and Vibration 362:228–251

Lindholm US, Kana DD, Chu WH, Abramson HN (1965) Elastic vibration characteristics of cantilever plates in water. Journal of Ship Research 9:11–22

Marcus MS (1978) A finite-element method applied to the vibration of submerged plates. Journal of Ship Research 22(2)

Melosh RJ (1963) Basis for derivation of matrices for the direct stiffness method. AIAA Journal 1(7):1631–1637

Meyerhoff WK (1970) Added masses of thin rectangular plates calculated from potential theory. J Ship Res 14:100–111

Meylan MH (1997) The forced vibration of a thin plate floating on an infinite liquid. Journal of sound and vibration 205(5):581–591

Motley MR, Kramer MR, Young YL (2013) Free surface and solid boundary effects on the free vibration of cantilevered composite plates. Composite structures 96:365–375

Rahali Y, Eremeyev VA, Ganghoffer JF (2020) Surface effects of network materials based on strain gradient homogenized media. Mathematics and Mechanics of Solids 25(2):389–406

Robinson NJ, Palmer SC (1990) A modal analysis of a rectangular plate floating on an incompressible liquid. Journal of sound and vibration 142(3):453–460

Vangelatos Z, Gu GX, Grigoropoulos CP (2019a) Architected metamaterials with tailored 3d buckling mechanisms at the microscale. Extreme Mechanics Letters 33:100,580

Vangelatos Z, Komvopoulos K, Grigoropoulos C (2019b) Vacancies for controlling the behavior of microstructured three-dimensional mechanical metamaterials. Mathematics and Mechanics of Solids 24(2):511–524

Vangelatos Z, Melissinaki V, Farsari M, Komvopoulos K, Grigoropoulos C (2019c) Intertwined microlattices greatly enhance the performance of mechanical metamaterials. Mathematics and Mechanics of Solids 24(8):2636–2648

Volcy GC, Baudin MM, Bereau MD (1980) Hydroelasticity and vibrations of internal steelwork of tanks. Tech. rep.

Warburton GB (1961) Vibration of a cylindrical shell in an acoustic medium. Journal of Mechanical Engineering Science 3(1):69–79

Yildizdag ME, Ardic IT, Demirtas M, Ergin A (2019) Hydroelastic vibration analysis of plates partially submerged in fluid with an isogeometric fe-be approach. Ocean Engineering 172:316–329

Zhang GJ, Li TY, Zhu X, Yang J, Miao YY (2017) Free and forced vibration characteristics of submerged finite elliptic cylindrical shell. Ocean Engineering 129:92–106

Zhang XM (2002) Frequency analysis of submerged cylindrical shells with the wave propagation approach. International Journal of Mechanical Sciences 44(7):1259–1273

Zhang XM, Liu GR, Lam KY (2001) The effects of baffles and end-caps on coupled vibration and sound radiation of finite cylindrical shells. Int J Eng Simulation 2:19–25

Zheng CJ, Zhang C, Bi CX, Gao HF, Du L, Chen HB (2017) Coupled fe–be method for eigenvalue analysis of elastic structures submerged in an infinite fluid domain. International Journal for Numerical Methods in Engineering 110(2):163–185

Zienkiewicz OC, Newton RE (1969) Coupled vibrations of a structure submerged in a compressible fluid. In: Symposium on Finite Element Techniques. Germany: Univ. of Stuttgart